Electronic Supplementary Material (ESI) for Soft Matter.

Supporting Information: Electric Polarizability of Metallodielectric Janus Particles in Electrolyte Solutions

Behrouz Behdani,† Kun Wang,† and Carlos A. Silvera Batista*,†,‡

†*Department of Chemical and Biomolecular Engineering, Vanderbilt University, Nashville, TN*
‡*Vanderbilt Institute for Nanoscale Science and Engineering*

E-mail: silvera.batista@vanderbilt.edu
Phone: (615) 875-6195

Effect of tagging on experimental results. The electrorotation experiments depend on the ability to quantify the angular velocity of the particles. For the JPs with thicker metal layers (15 and 35 nm), visualization is straightforward due to the contrast from the metal layer. However, for JP-5 nm and non-patchy silica particles, visualization is more challenging due to the lack of contrast. To overcome that challenge, JPs are tagged with fluorescent particles, as described in the main text. To make sure that the tagging does not change the response of the particles appreciably, we compare the angular velocity of particles (JP-15 nm) with and without tags in Figure S1. The data shows that tagging, as perform in our experiments, does dot affect the response of the particles. Except for minor differences, the angular velocity for the two sets of particles is the same, when the spread in the data is accounted for.

Dependence of angular velocity with strength of electric field. The angular velocity was measured when different voltages were applied. The results of the measurements are shown in Figure S2. The linear dependence with the squared of the voltage indicates the electric field inter-

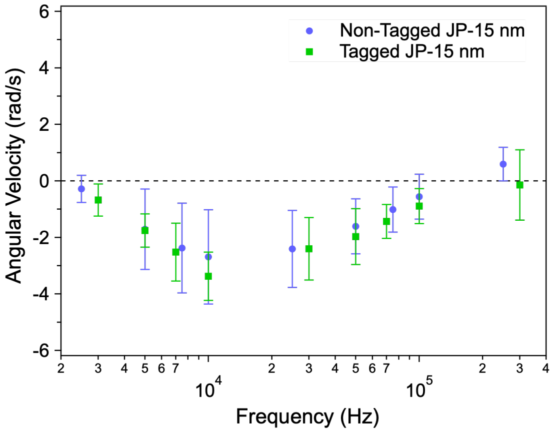

Figure S1: Comparison of angular velocity for JP-15 nm with and without fluorescent tags in DI water. The data shows that tagging, as performed in this work, did not affect the basic properties of JPs.

acts with charges and dipoles that are induced by the field itself.

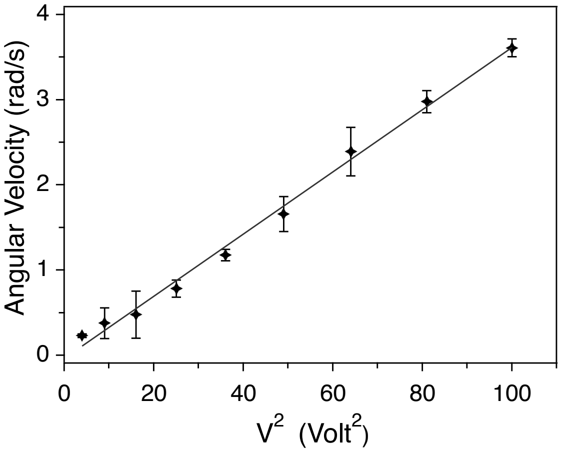

Figure S2: Dependence of angular velocity on strength of electric field at 50 kHz. The dependence of angular velocity on the square of the magnitude of electric field implies that rotation is due to the interaction of the electric field with the charges induced by the field itself.

Comparison of the angular velocity from simulations and experiments. Figure S7 shows the angular velocity derived from the calculations of $Im[B(\omega)]$ and from a modified version of equation 3 (main text) that accounts for the higher friction near the glass substrate,

$$\Omega = -\frac{\varepsilon E_0^2}{4\eta\xi} \cdot \mathrm{Im}\left[A(\omega) + B(\omega)\right]. \tag{1}$$

ξ stands for the correction factor, with an approximate value of 1.20206.[S1,S2] The conversion to angular velocity was performed using a value of 30 kV/m for the electric field. This value is on the upper limit, so realistically, the average value at the center of the electrode array is likely to be lower.

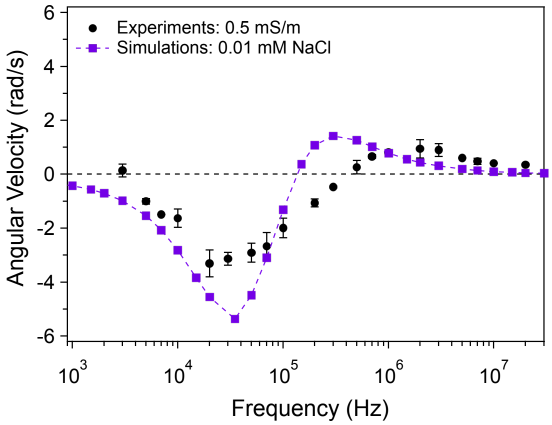

Figure S3: Comparison of the angular velocity measured in experiments and the values calculated from Equation 3 in the main text. The calculated values were adjusted to account for the higher friction coefficient close to the glass substrate. The calculations provide values for angular velocity that are reasonable in comparison to the experimentally measured values.

Heat and vector maps describing polarization of metal and Janus particles.

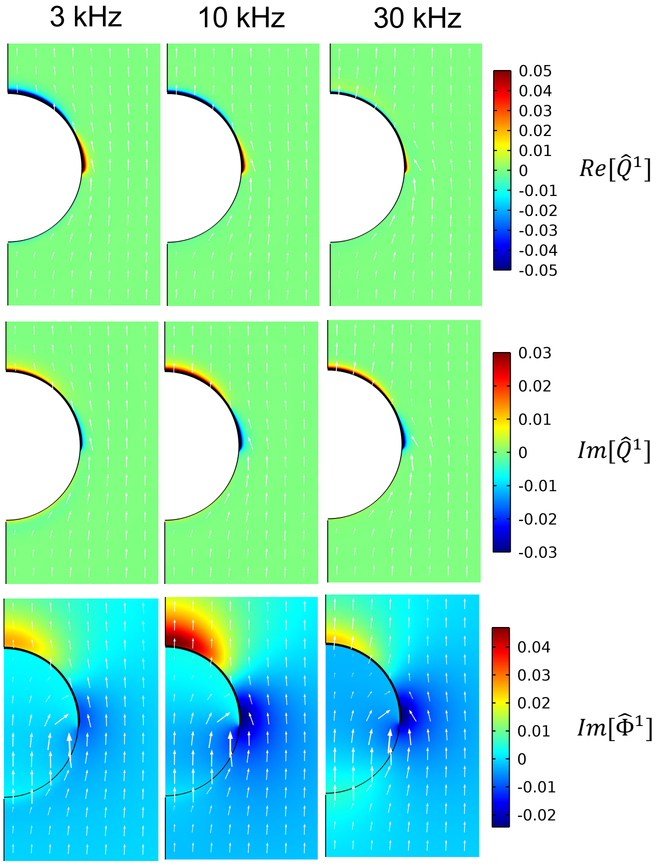

Figure S4: Heat and vector maps representing different quantities for JP-35 nm in 0.01 mM NaCl. The top row represents the real part of the dimensionless perturbation for charge density, $Re[\hat{Q}^1]$; the center row shows the complex part of the dimensionless perturbation for charge density, $Im[\hat{Q}^1]$; the bottom row shows the complex part of the scaled potential $Im[\hat{\phi}^1]$ and electric field.

Plots of the charge density for JPs and metal particles provide insight into the frequency dependent polarization of JPs (Figures S5 and S6). The metal hemisphere of Janus particles resembles

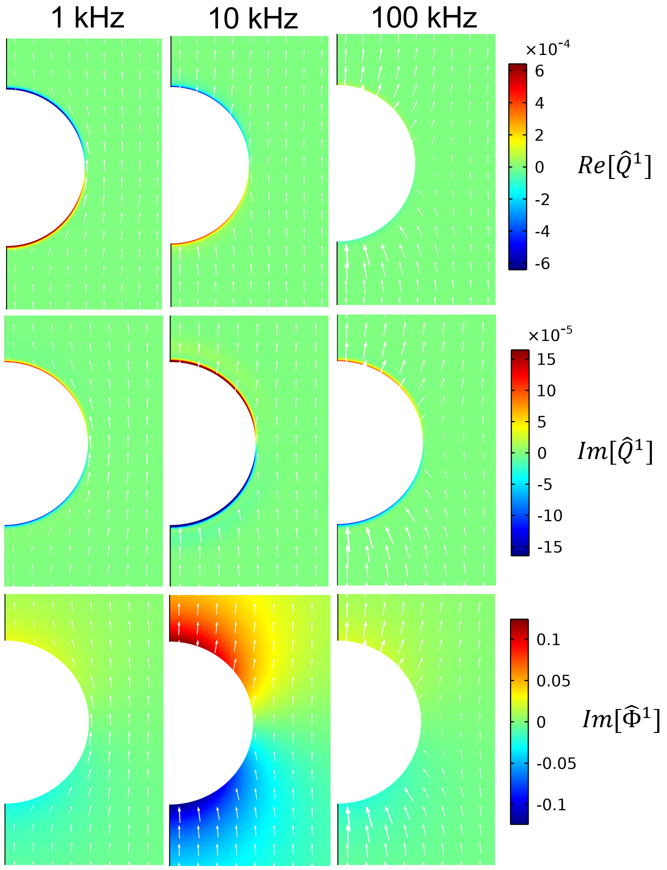

Figure S5: Heat and vector maps representing different quantities for metal particles ($r = 1.8\ \mu$m) in 0.1 mM NaCl. The top row represents the real part of the dimensionless perturbation for charge density, $Re[\hat{Q}^1]$; the center row shows the complex part of the dimensionless perturbation for charge density, $Im[\hat{Q}^1]$; the bottom row shows the complex part of the scaled potential $Im[\hat{\phi}^1]$ and electric field.

the behavior of fully metal particles. In the absence of electron transfer reactions and when driven by an external electric field, ions accumulate at the metal-electrolyte interface, leading to the formation of a diffuse double layer.[S3,S4] The RC time represents the characteristic scale for charging the double layer, and based on the Debye-Huckle theory, it is given by $\tau_{RC} = \frac{2\pi\varepsilon_m a}{\sigma_m \lambda_D}$. σ_m stands for the bulk conductivity of the medium. Peaks in angular velocity are expected at frequencies (≈ 10 kHz) that scale with the inverse of the RC time in the liquid.[S4] From the perspective of an outside observer, metal particles behave as insulators at low frequencies, since the electrical double layer has enough time to charge. In this case, the electric field lines pass around the particles with minimal perturbation (Figure S5). At high frequencies, the component of charge density in phase with the field decreases substantially, while the component out of phase with the field increases rapidly. At this point, metal particles display a relaxation. The complex part of the perturbed potential signals the occurrence of the relaxation clearly.

Effect of surface charge on the response at high frequencies. Figure S6 shows imaginary component of the dipole coefficient ($Im[K(\omega)]$), calculated using the PNP model for a silica sphere, 3.6 μm in diameter. The dipole coefficient $K(\omega)$ for a non-patchy sphere is extracted from the following expression,

$$\tilde{\mathbf{p}} = 4\pi\varepsilon r^3 K(\omega)\mathbf{E}. \tag{2}$$

The model reveals the relaxation at high frequencies to be quite sensitive to the zeta potential or surface charge of the particles. For solutions of constant NaCl concentration (0.1 mM), the magnitude of the peak at 300 kHz increases with decreasing zeta potential.

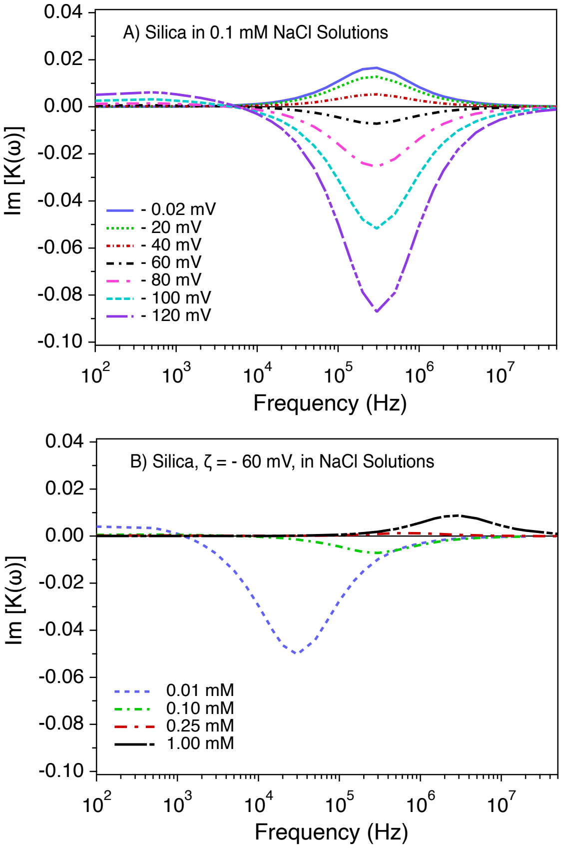

Figure S6: Magnitude of the imaginary part of the dipole coefficient, calculated from the electrokinetic model for a non-patchy silica particle with $r = 1.8$ μm. The calculation was performed using the diffusivity values for NaCl at similar concentrations as in the experiments. Notice that a negative dipole coefficient implies cofield rotation, according to Equation 3 (main text). A) Results for different values of ζ in 0.1 mM NaCl. B) Results for different values of NaCl concentration, with $\zeta = -60$ mV.

Furthermore, the value of $Im[K(\omega)]$ transitions from negative to positive values with increasing zeta potential. A significantly high magnitude of zeta potential ($|\zeta| > 40mV$) becomes necessary to observe cofield rotation. For low magnitude of zeta potential, the particles will experience counterfield rotation as predicted from the Maxwell-Wagner model. For a particle with a fixed zeta potential (-60 mV), the model also captures the behavior at different concentrations of NaCl. First, the frequency of the relaxations shifts to higher values as the concentration of NaCl increases, while the magnitude of the dipole coefficients decreases until there is a crossover from negative to positive values. Interestingly, the imaginary component of the dipole coefficient reach values close to zero at all frequencies for a concentration of 0.25 mM. A similar feature was observed in the experiments, although at a higher concentration of NaCl. The modelling work by Grosse and collaborators have produced similar trends for charged polystyrene particles.[S5]

Polarization of Janus particles as a function of κr.

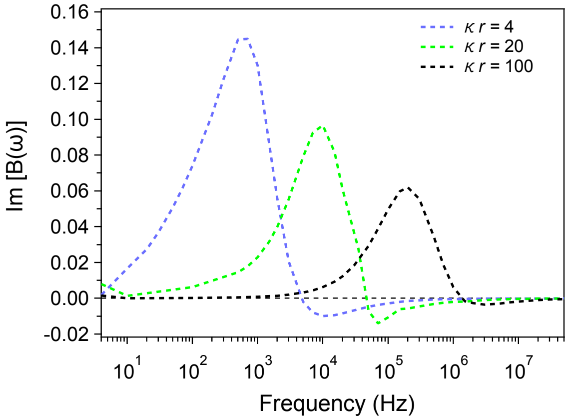

Figure S7: As the value of κr decreases, the model predict a shift to lower frequencies for both peaks. The magnitude of the first peak increases as observed in the experiments. This data is complementary to the effect of conductivity, in Figures 6 and S6. κ is the inverse of the Debye length.

References

(S1) Rodríguez-Sánchez, L.; Ramos, A.; García-Sánchez, P. Electrorotation of semiconducting microspheres. *Physical Review E* **2019**, *100*, 042616.

(S2) García-Sánchez, P.; Ren, Y.; Arcenegui, J. J.; Morgan, H.; Ramos, A. Alternating Current Electrokinetic Properties of Gold-Coated Microspheres. *Langmuir* **2012**, *28*, 13861–13870.

(S3) García-Sánchez, P.; Ramos, A. Electrorotation of a metal sphere immersed in an electrolyte of finite Debye length. *Physical Review E* **2015**, *92*, 052313.

(S4) Ren, Y. K.; Morganti, D.; Jiang, H. Y.; Ramos, A.; Morgan, H. Electrorotation of Metallic Microspheres. *Langmuir* **2011**, *27*, 2128 – 2131.

(S5) Zimmerman, V.; Shilov, V. N.; López-García, J. J.; Grosse, C. Numerical Calculation of the Electrorotation Velocity of Latex-Type Particles. *The Journal of Physical Chemistry B* **2002**, *106*, 13384–13392.